

ExoMol molecular line lists - XXVI: spectra of SH and NS

Sergei N. Yurchenko¹, Wesley Bond¹, Maire N. Gorman^{1,2}, Lorenzo Lodi¹,
 Laura K. McKemmish¹, William Nunn¹, Rohan Shah¹ and Jonathan Tennyson^{1*}

¹ Department of Physics and Astronomy, University College London, London WC1E 6BT, UK

² Department of Physics, Aberystwyth University, Penllais, Aberystwyth, Ceredigion, UK, SY23 3BZ

Accepted XXXX. Received XXXX; in original form XXXX

ABSTRACT

Line lists for the sulphur-containing molecules SH (the mercapto radical) and NS are computed as part of the ExoMol project. These line lists consider transitions within the $X^2\Pi$ ground state for ^{32}SH , ^{33}SH , ^{34}SH and ^{32}SD , and $^{14}\text{N}^{32}\text{S}$, $^{14}\text{N}^{33}\text{S}$, $^{14}\text{N}^{34}\text{S}$, $^{14}\text{N}^{36}\text{S}$ and $^{15}\text{N}^{32}\text{S}$. *Ab initio* potential energy (PEC) and spin-orbit coupling (SOC) curves are computed and then improved by fitting to experimentally observed transitions. Fully *ab initio* dipole moment curves (DMCs) computed at high level of theory are used to produce the final line lists. For SH, our fit gives a root-mean-square (rms) error of 0.03 cm^{-1} between the observed ($v_{\text{max}} = 4$, $J_{\text{max}} = 34.5$) and calculated transitions wavenumbers; this is extrapolated such that all $X^2\Pi$ rotational-vibrational-electronic (rovibronic) bound states are considered. For ^{32}SH the resulting line list contains about 81 000 transitions and 2 300 rovibronic states, considering levels up to $v_{\text{max}} = 14$ and $J_{\text{max}} = 60.5$. For NS the refinement used a combination of experimentally determined frequencies and energy levels and led to an rms fitting error of 0.002 cm^{-1} . Each NS calculated line list includes around 2.8 million transitions and 31 000 rovibronic states with a vibrational range up to $v = 53$ and rotational range to $J = 235.5$, which covers up to $23\,000\text{ cm}^{-1}$. Both line lists should be complete for temperatures up to 5000 K. Example spectra simulated using this line list are shown and comparisons made to the existing data in the CDMS database. The line lists are available from the CDS (<http://cdsarc.u-strasbg.fr>) and ExoMol (www.exomol.com) data bases.

Key words: molecular data; opacity; astronomical data bases: miscellaneous; planets and satellites: atmospheres; stars: low-mass

1 INTRODUCTION

Sulphur chemistry is important in a variety of astronomical environments including the interstellar medium (ISM) (Oppenheimer & Dalgarno 1974; Duley et al. 1980; Vidal et al. 2017), hot cores (Charnley 1997; Woods et al. 2015), comets (Canaves et al. 2002; Rodgers & Charnley 2006; Canaves et al. 2007), starburst and other galaxies (Martín et al. 2005; Martín 2005), exoplanets (Visscher et al. 2006; Zahnle et al. 2009), and brown dwarfs and low-mass dwarf stars (Visscher et al. 2006). The ExoMol project aims at providing comprehensive molecular line lists for exoplanet and other atmospheres. ExoMol has provided line lists for several sulphur-bearing molecules: CS (Paulose et al. 2015), SO₂ (Underwood et al. 2016a), H₂S (Azzam et al. 2016), SO₃ (Underwood et al. 2016b), and PS (Prajapat et al. 2017); a line list for SiS has also just been completed (Upadhyay et al. 2018). In this work we extend this coverage by providing line lists for the major isotopologues of SH and NS. For both species we only consider transitions within the ground electronic state: both SH and NS have an $X^2\Pi$ ground state. The excited electronic states lie above $30,000\text{ cm}^{-1}$ and $23,000\text{ cm}^{-1}$ for SH and NS, respectively, and thus the line lists presented here will be accurate for the visible, infrared and radio spectral regions. Both species are well-known astronomically from transitions within the ground state.

* Email: j.tennyson@ucl.ac.uk

The diatomic mercapto radical SH has long been of interest to astronomers, but proved challenging to detect. It was definitively detected in the interstellar medium (ISM) (Neufeld et al. 2012), in asymptotic-giant-branch (AGB) stars (Yamamura et al. 2000) and the Sun’s atmosphere (Berdyugina & Livingston 2002), tentatively detected in comets (Krishna Swamy & Wa 1987, 1988) and predicted to occur in brown dwarfs (Visscher et al. 2006) and hot Jupiter exoplanets (Visscher et al. 2006; Zahnle et al. 2009) as one of the major sulphur-bearing gases after H₂S. The ISM detection was difficult due to the location of the key rotational transition which was inaccessible both from the ground and the Herschel telescope; after a number of failed searches in the ISM (Meeks et al. 1969; Heiles & Turner 1971), Neufeld et al. (2012) finally detected SH in the terahertz region using SOFIA (Stratospheric Observatory For Infrared Astronomy) by its 1383 GHz ${}^2\Pi_{3/2}$ $J = \frac{5}{2} - \frac{3}{2}$ transition. The $A\ {}^2\Sigma^+ - X\ {}^2\Pi$ band, a UV absorption band not considered in this paper, has also been used to detect SH in translucent interstellar clouds (Zhao et al. 2015) and in the Sun’s atmosphere (Berdyugina & Livingston 2002). Zahnle et al. (2009) generated an $A-X$ line list for SH.

In our own atmosphere, SH is known to react with NO₂, O₂ and O₃; SH is produced in the troposphere by oxidation of H₂S by the OH radical (Ravichandran et al. 1994).

Experimentally, SH spectra have been studied since 1939 (Glockler & Horwitz 1939; Lewis & White 1939) with over 100 experimental publications to date. This work is based on the measured transitions from experimental studies presented in Table 1.

A number of multi-reference configuration interaction (MRCI) level theoretical calculations have been performed on SH (Raimondi et al. 1975; Hirst & Guest 1982; Bruna & Hirsch 1987), with the most recent study been those of Kashinski et al. (2017) and Vamhindi & Nsangou (2016). Spin-orbit splitting of the ground state potential energy curve (PEC) was calculated by Baeck & Lee (1990) and Qui-Xia et al. (2008). Lifetimes for SH have previously been calculated by McCoy (1998) and Brites et al. (2008) with Resende & Ornellas (2001).

Transitions for NS are much more astronomically accessible and it was one of the first ten diatomic molecules to be detected in space (Somerville 1977; Lovas et al. 1979), with the first positive detection by Gottlieb et al. (1975) using the $J = 5/2 - 3/2$ transition of the ${}^2\Pi_{1/2}$ state at 115.6 GHz towards Sagittarius B2. Radio astronomy has also been used to detect NS in giant molecular clouds (McGonagle et al. 1992; Leurini et al. 2006; Belloche et al. 2013), cold dark clouds (McGonagle et al. 1994), comets (Irvine et al. 1999; Biver 2005), extragalactically (Martín et al. 2003) and the NGC 253 starburst region Meier et al. (2015).

Experimentally, there have been significant experimental work focusing on the excited electronic states; however, this is not of relevance to this work. Numerous experimental studies on NS have been made on the spectra of the ground state. Laser magnetic resonance (LMR) studies include those of Carrington et al. (1968), Uehara & Morino (1969), Anaconda (1994) and Anaconda (1995). Experimental measurements of rovibrational transitions within the ground state are reported in a series of papers (Narasimham & Balasubramanian 1971; Matsumura et al. 1980; Lovas & Suenram 1982; Anaconda et al. 1986; Sinha et al. 1988; Lee et al. 1995; Amano et al. 1969). The experimental frequencies used in this work are summarised in Table 2.

Early electronic structure calculation on NS were made by Bialski & Grein (1976), Salahub & Messmer (1976) and Karpfen et al. (1978). Subsequently, Lie et al. (1985) and Karna & Grein (1986) performed configuration interaction studies on the low-lying and Rydberg states of NS. CCSD(T) calculation of equilibrium geometries of NS for plasma applications were made by Czernek & Živný (2004). The most recent theoretical study on NS is that of Gao et al. (2013) who undertook calculations at the MRCI+Q+DK/AV5Z level of theory for the PECs of low-lying electronic states. However, while there are some computed dipole moment (Lie et al. 1985; Gao et al. 2013) and spin-orbit coupling (Shi et al. 2012) curves, we perform new *ab initio* calculations to ensure the uniform quality of our model.

2 METHOD AND SPECTROSCOPIC MODELS

Our general method is to start from high quality *ab initio* potential energy curves (PECs), associated coupling curves and dipole moment curves (DMCs). Since *ab initio* transition frequencies are not accurate enough, the PECs and couplings are refined using empirical energy levels and transition wavenumbers from laboratory spectra. *Ab initio* DMCs are found to give the best results. The nuclear motion problem is solved using the program Duo (Yurchenko et al. 2016a) which allows for full couplings between the curves, see Tennyson et al. (2016b) for a full discussion of the theory. DUO has been successfully used to produce line lists for a number of diatomic molecules AlO, PS, PN, ScH, VO, NO, CaO, SiH (Patrascu et al. 2015; Lodi et al. 2015; McKemmish et al. 2016; Yurchenko et al. 2016b; Wong et al. 2017; Prajapat et al. 2017; Yurchenko et al. 2018). The refined PECs, coupling curves and DMCs together form a spectroscopic model for the diatomic system, which can be useful beyond the immediate line list application considered here.

Both SH and NS have $X\ {}^2\Pi$ ground states. In this case the spin-orbit (SO) coupling splits the PEC in two curves, which are often denoted ${}^2\Pi_{3/2}$ and ${}^2\Pi_{1/2}$. The SO splitting coupling presents a significant contributions to the energies of these molecules:

360 cm⁻¹ and 220 cm⁻¹ for the $v = 0$ states of SH and NS, respectively. Another important coupling for spectroscopy of the $^2\Pi$ systems is the due to the presence of electronic angular momentum (EAM), which causes the Λ -doubling effect.

We use the extended Morse oscillator (EMO) functions (Lee et al. 1999) to represent the PECs, both *ab initio* and refined. In this case the PEC is given by

$$V(r) = V_e + (A_e - V_e) \left[1 - \exp \left(- \sum_{k=0}^N B_k \xi_p^k (r - r_e) \right) \right]^2, \quad (1)$$

where $A_e - V_e$ is the dissociation energy, r_e is an equilibrium distance of the PEC, and ξ_p is the Šurkus variable given by:

$$\xi_p = \frac{r^p - r_e^p}{r^p + r_e^p}. \quad (2)$$

The corresponding expansion parameters are obtained by fitting to the experimental data (energies and frequencies) of the molecule in question, as detailed below.

To model the SO coupling we use *ab initio* curves computed using high levels of theory with the program MOLPRO (Werner et al. 2012). These curves are then refined by fitting to the experimental data using the morphing approach (Meuwly & Hutson 1999; Skokov et al. 1999). In this approach, the *ab initio* curves represented on a grid of bond lengths are ‘morphed’ using the following expansion:

$$F(r) = \sum_{k=0}^N B_k z^k (1 - \xi_p) + \xi_p B_\infty, \quad (3)$$

where z is either taken as the Šurkus variable $z = \xi_p$ or the damped-coordinate given by:

$$z = (r - r_{\text{ref}}) e^{-\beta_2(r - r_{\text{ref}})^2 - \beta_4(r - r_{\text{ref}})^4}, \quad (4)$$

see also Prajapat et al. (2017) and Yurchenko et al. (2018). Here r_{ref} is a reference position equal to r_e by default and β_2 and β_4 are damping factors. When used for morphing, the parameter B_∞ is usually fixed to 1.

The Λ -doubling effects in DUO can be modelled directly using an effective Λ -doubling function, in case of $^2\Pi$ we use the $(p + 2q)$ effective coupling (Brown & Merer 1979) given by:

$$\hat{H}_{\text{LD}} = -\frac{1}{2} \alpha_{p2q}^{\text{LD}}(r) \left(\hat{J}_+ \hat{S}_+ + \hat{J}_- \hat{S}_- \right). \quad (5)$$

\hat{H}_{LD} leads to a linear \hat{J} -dependence, which is justified for the heavy molecule like NS. In this case for $\alpha_{p2q}^{\text{LD}}(r)$ we use a simple, one-parameter function:

$$\alpha_{p2q}^{\text{LD}} = B_0^{p2q} (1 - \xi_p). \quad (6)$$

For the SH molecule, which is affected by a stronger centrifugal distortion, this is not appropriate. Here we follow the approach recently used for solving another hydrogen-containing $^2\Pi$ system, SiH (Yurchenko et al. 2018), where the Λ -doubling is modelled via an EAM interaction with a closely lying $^2\Sigma$ -state (Brown & Merer 1979). In the case of $X \ ^2\Pi$ of SH, the closest Σ state is $A \ ^2\Sigma^-$. The latter is introduced with a dummy potential curved in the EMO representation, while the EAM-curve is given by the 1st order ξ_p -type expansion in Eq. (3) (see also below).

The dipole moment curves (DMC) of SH and NS are computed using a high level *ab initio* theory on a grid of bond length values ranging from about 0.8 to 8 Å. In order to reduce the numerical noise in the intensity calculations of high overtones (see recent recommendations by Medvedev et al. (2016) the DMCs are represented analytically. The expansion with a damped z coordinate in Eq. (3) is employed (Prajapat et al. 2017; Yurchenko et al. 2018).

All these functional forms are included in DUO (functions.f90). The corresponding expansion parameters as well as their grid representations can be found in the DUO input files provided as supplementary data.

2.1 SH

The DUO model for SH consists of two PECs, $X \ ^2\Pi$ and $A \ ^2\Sigma^+$, represented by EMO forms in Eq. (1), diagonal ($X-X$) and non-diagonal ($X-A$) SO coupling curves (*ab initio*) morphed by functions using Eq. (3), an EAM coupling curve ($X-A$) also represented by Eq. (3), and by a diagonal $X-X$ DMC. The A state PEC is only used to support the Λ -doubling effect in the X -state energies and is not included in SH the line list. We use the *ab initio* SO coupling curves obtained at the MRCI+DKH4+Q level of theory, where DKH4 is the fourth-order Douglas-Kroll-Hess representation of the relativistic Hamiltonian and Q denotes a Davidson correction. An AWC5Z Gaussian Type basis set was used (Dunning Jr. 1989; Woon & Dunning 1993; Peterson & Dunning Jr. 2002; Szalay et al. 2012). The *ab initio* PE, SO, EAM and DM curves of SH used in this work are shown in Figs 1–4.

The PEC, SO and EAM expansion parameters were obtained by fitting to the experimental frequencies from the sources listed in Table 1 with a root-mean-square (rms) error of 0.03 cm⁻¹. The empirical vibrational information is limited to only $\Delta v = 0$ and $\Delta v = 1$ transitions with $v_{\text{max}} = 4$, which complicates obtaining a globally accurate model from the fitting. The

Table 1. List of experimental data used in refinement of the SH $X^2\Pi$ potential energy curves.

Source	No. of transitions	Vibrational bands	J_{\max}
Bernath et al. (1983)	50	(1-0)	11.5
Winkel & Davis (1984)	285	(1-0), (2-1), (3-2)	34.5
Ram et al. (1995)	175	(1-0), (2-1), (3-2), (4-3)	16.5
Yamamura et al. (2000)	30	(1-0), (2-1), (3-2)	25.5
Eliet et al. (2011)	6	(0-0)	4.5
Martin-Drumel et al. (2012)	70	(0-0), (1-1)	16.5

Table 2. Experimental sources of NS spectroscopic data used in the refinement of the PEC. FTS=Fourier Transform Spectrometry, WS=millimetre and sub-millimetre Wave spectrometry.

Study	Method	J	ν	Range (cm^{-1})
Anaconda et al. (1986)	WS	2.5 – 6.5	(v, v), $v \leq 5$	2.3 – 10.1
Sinha et al. (1988)	FTS	0.5 – 35.5	(1, 0)	1,149 – 1,251
Lee et al. (1995)	WS	0.5 – 7.5	(0,0)	2.3 – 11.6

Table 3. Example of Observed – Calculated residuals for SH frequencies as a function of J for the (0, 0) band where $J' = J'' + 1$.

J	+/-	Ω	Obs.	Calc.	Obs.-Calc.
1.5	-	1.5	46.1289	46.1293	-0.0004
2.5	+	1.5	64.5513	64.5519	-0.0006
3.5	-	0.5	86.8367	86.8418	-0.0051
3.5	+	1.5	82.9811	82.9808	0.0003
4.5	-	0.5	106.2538	106.2508	0.0030
5.5	-	1.5	119.6169	119.6179	-0.0010
6.5	+	1.5	137.8762	137.8771	-0.0009
7.5	+	1.5	156.1850	156.1846	0.0004
8.5	-	0.5	181.9686	181.9684	0.0002
9.5	+	0.5	200.5907	200.5909	-0.0002
10.5	-	0.5	219.0671	219.0677	-0.0006
11.5	+	1.5	228.2230	228.2231	-0.0001
12.5	-	0.5	255.5412	255.5415	-0.0003
13.5	-	0.5	273.5067	273.5068	-0.0001
14.5	-	1.5	281.0630	281.0639	-0.0009
15.5	+	1.5	298.3891	298.3901	-0.0010

refined curves are shown in Figs 1–3. The quality of the fit is illustrated in Fig. 5, where the Obs.–Calc. residuals for all experimental data are shown and in Tables 3 and 4. Most of the $\Delta v = 0$ ($v_{\max} = 4$) and $\Delta v = 1$ ($v_{\max} = 1$) frequencies are reproduced within 0.005 cm^{-1} , except for the $\Pi_{3/2}$ band, which is found to diverge at $J = 25$ by about 0.15 cm^{-1} . Our final value for D_e (4.46 eV), corresponding to the best fit, is higher than the experimental $X^2\Pi$ dissociation energy of $3.62 \pm 0.03 \text{ eV}$ (D_0) by Continetti et al. (1991), as well as with the *ab initio* values recommended by Csaszar et al. (2003) $D_e = 3.791 \text{ eV}$ and $D_0 = 3.625 \text{ eV}$. Therefore we limit our extrapolations to high vibrational excitations to those that do not to exceed this D_0 value.

The final spectroscopic model (provided as a DUO input file in the supplementary material) was then used to generate line lists for the following isotopologues: ^{32}SH , ^{33}H , ^{34}H , ^{36}SH ($J_{\max} = 64.5$) and ^{32}SD ($J_{\max} = 89.5$). In the DUO calculations we used a sinc DVR method based on the grid of 501 points equally distributed from 0.85 to 5.0 Å. The equilibrium value of the *ab initio* (MRCI/AWC5Z) dipole moment of SH ($X^2\Pi$) is $\mu_e = 0.801 \text{ D}$ (at $r = 1.3565 \text{ Å}$). The vibrationally averaged dipole moments, given by $\mu_v = \langle v | \mu | v \rangle$ where $|v\rangle$ is the vibrational eigenfunction of $X^2\Pi$ at the limit of $J = 0$, are $\mu_0 = 0.794 \text{ D}$ and $\mu_1 = -0.017 \text{ D}$.

The experimental value of the SH ($v = 0$) dipole moment of 0.7580(1) D was obtained by Meerts & Dymanus (1974) in a Stark experiment. Benidar et al. (1991) reported anomalously weak intensities of the fundamental band of SH and obtained a very rough estimate for a relative dipole moment value of $|\mu_1|/|\mu_0|$ of $(0.011 \pm 0.016 \text{ D})/0.63 \text{ D} = 0.017 \pm 0.023$, which compares favourably to our value $|\mu_1|/|\mu_0| = 0.027$.

2.2 NS

The electronic structure of the lowest seven states of NS was intensely studied by Gao et al. (2013). In this work we only concentrate on the ground electronic state spectrum of NS. The program MOLPRO (Werner et al. 2012) was used to compute *ab initio* PEC, SOC and DMC for the NS $X^2\Pi$ ground state along with the spin-orbit coupling curve for this state on a grid

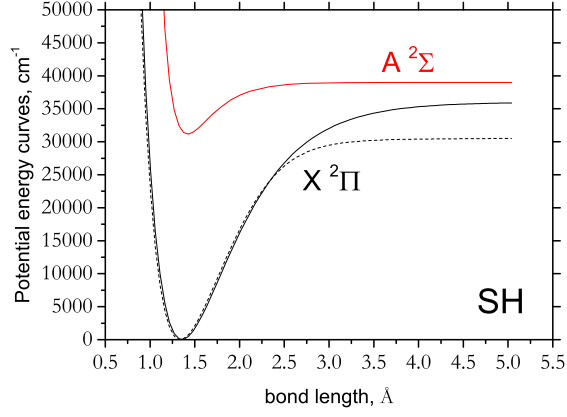


Figure 1. Potential energy curves of SH: fitted (solid) and *ab initio* (dashed).

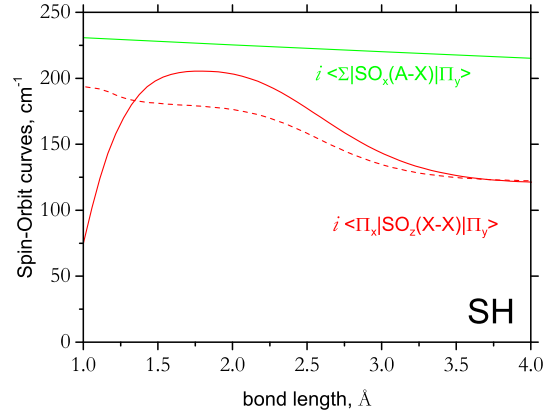


Figure 2. Spin-orbit curves of SH: X-X, fitted (solid) and *ab initio* (dashed) and A-X, fitted only (solid).

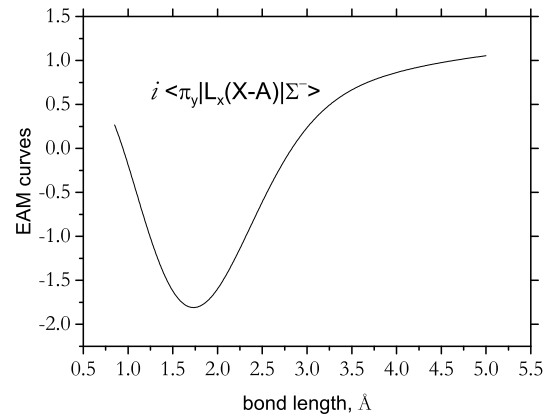
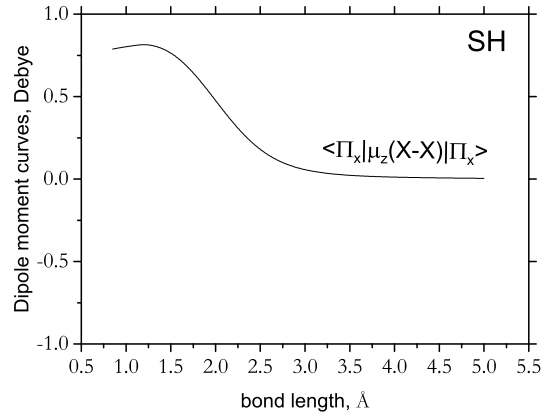
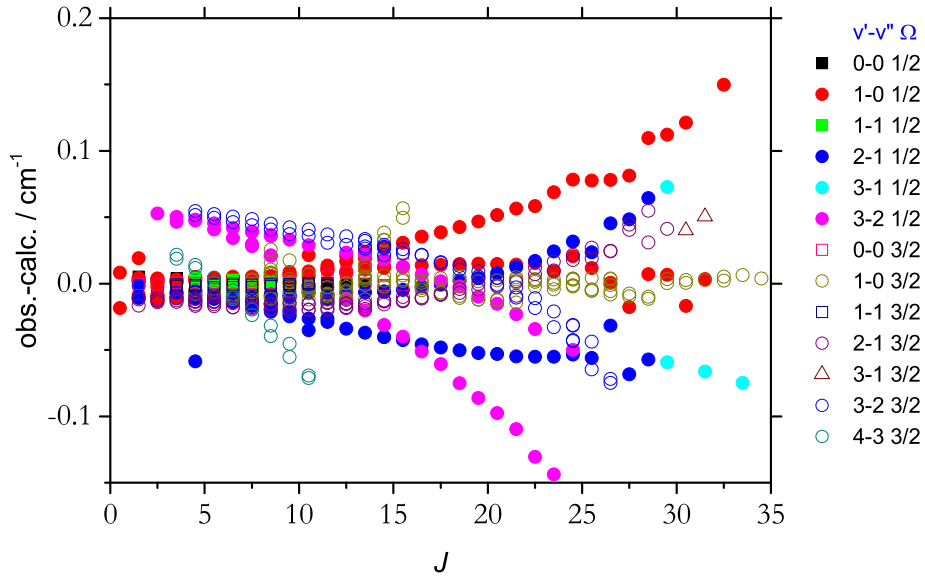


Figure 3. An empirical EAM curve (A-X) of SH.

Table 4. Example of Observed – Calculate residuals for SH frequencies for various vibrational bands as a function of J where $J' = J'' + 1$.

J	+/-	Ω	Band	Obs.	Calc.	Obs.-Calc.
1.5	+	0.5	(0, 0)	48.5370	48.5318	0.0052
1.5	-	1.5	(1, 0)	2642.8296	2642.8262	0.0034
1.5	+	0.5	(1, 0)	2644.8974	2644.8939	0.0035
3.5	-	1.5	(1, 1)	80.5572	80.5590	-0.0018
3.5	+	1.5	(1, 1)	80.5901	80.5907	-0.0006
1.5	-	0.5	(2, 1)	2546.2628	2546.2735	-0.0107
1.5	+	1.5	(2, 1)	2544.5747	2544.5867	-0.0120
2.5	-	0.5	(3, 2)	2464.0678	2464.0150	0.0528
3.5	-	0.5	(3, 2)	2479.3627	2479.3160	0.0467
3.5	-	1.5	(4, 3)	2376.6704	2376.6516	0.0188
3.5	+	1.5	(4, 3)	2376.6944	2376.6727	0.0217

**Figure 4.** The diagonal $X^2\Pi$ *ab initio* dipole moment curve of SH.**Figure 5.** Observed – Calculated residuals for SH.

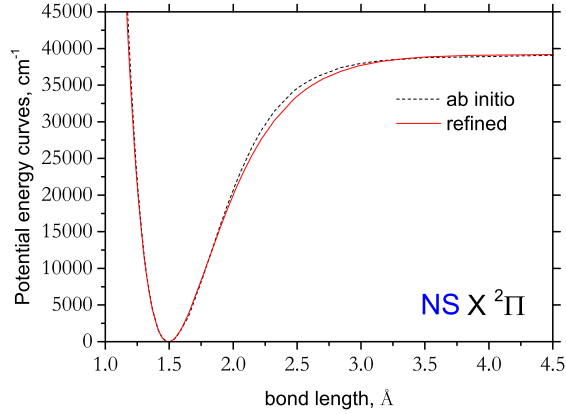


Figure 6. *Ab initio* PEC and refined PEC for the $X^2\Pi$ state of NS, see Eq. (1).

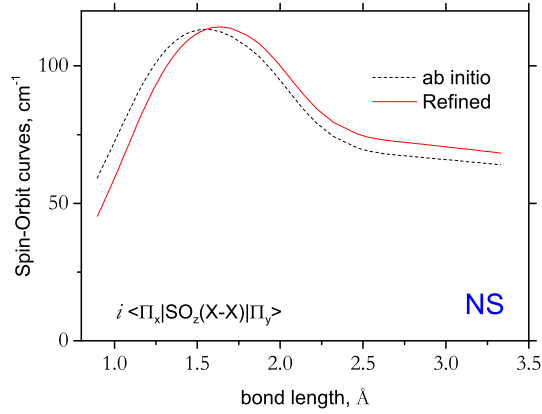


Figure 7. *Ab initio* and refined SO curves of NS.

of 143 geometries distributed between 0.8 Å and 2.7 Å using the MRCI method and Douglas-Kroll Hamiltonian (dkroll=2) with an aug-cc-pVQZ-DK basis set and the Davidson correction included. The (2s,2p)/N and (2s,2p)/O complete active space (CAS) is defined by 8330/4110 in the C_{2v} symmetry employed by MOLPRO.

The *ab initio* PEC, SO and DMC are shown in Figs. 6–8. The *ab initio* DMC of NS was modelled using the damped-variable expansion in Eq. (3). The equilibrium dipole value μ_e is 1.834 D (at $r_e = 1.494$ Å), while the vibrationally averaged μ_0 is 1.825 D, which is in a good agreement with the experimental (Stark) value of 1.81 D due to Amano et al. (1969).

In order to fit the PEC and SO curves of NS to the experimental data for the $X^2\Pi$ state, several steps were taken. Firstly, the program PGOPHER (Western 2017) was used to construct a list of rovibronic energies using the molecular parameters published by Sinha et al. (1988). The MARVEL procedure (Furtenbacher et al. 2007) was then used to transform the list of measured experimental transitions summarised in Table 2 into several ‘networks’ of derived energies: these were used to check the rovibronic energies determined using PGOPHER. This list of experimentally derived energies was then used to perform an initial fit of the data, which was then improved by using the actual experimentally measured frequencies.

The DUO calculations were based on the sinc DVR method comprising 701 points evenly distributed between 0.9 Å and 3.3 Å. The *ab initio* $X^2\Pi$ PEC of NS was represented using the EMO form in Eq. (1) and refined by fitting to 358 experimental frequencies covering the rotational excitations up to $J = 32.5$ and vibrational states up to $v = 5$; however, only $v = 1 - 0$ transitions are for an the vibration band, the remaining are microwave transitions for which $\Delta v = 0$.

In the fits, we also included the 161 PGOPHER term values ($J \leq 23.5$) generated from the constants by Sinha et al. (1988). Using experimentally-derived energies together with the measured frequencies helps to constrain the fitted value to the absolute energies, not only to the separation between them. This tends to make fits more stable and prevent drifts between states (see also Patrascu et al. (2015)). In the refinement, the effects of the spin-orbit coupling and Λ -doubling were taken

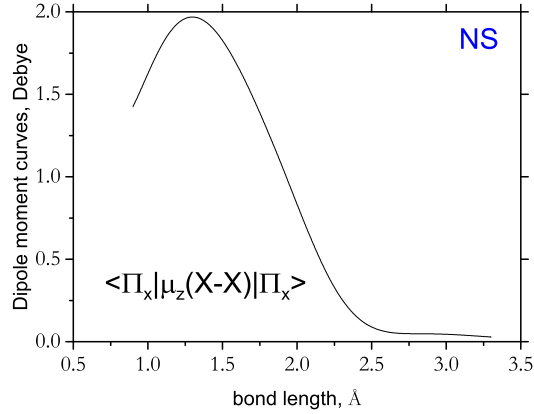


Figure 8. *ab initio* Dipole moment Curve of NS.

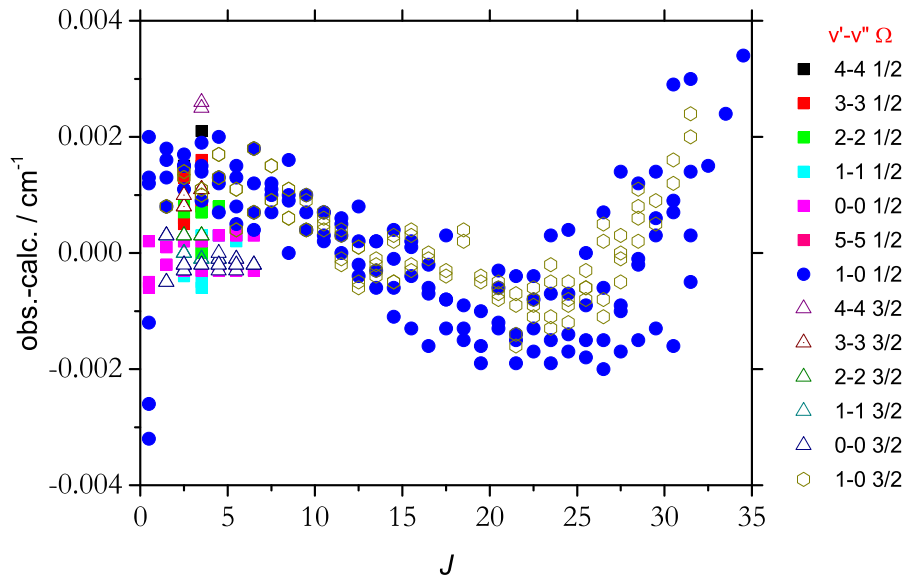


Figure 9. Observed – Calculated residuals for NS.

into account: the *ab initio* SOC was morphed and the Λ -doubling curves was refined by using the expression in Eq. (3). The refined PEC and SOC of NS are shown in Figs. 6 and 7. The fitted parameters are presented in the supplementary material.

Our final model reproduces the experimental frequencies with an rms error of 0.002 cm^{-1} . The experimentally derived energies are reproduced with an rms error of 0.03 cm^{-1} . Fig.9 shows the difference between the transition frequencies (cm^{-1}) calculated using the refined curves (Calc.) and those experimentally measured (Obs.). The error for most of the data is within 0.002 cm^{-1} , which is comparable to that obtained by the effective rotational methods. Table 5 shows a sample of the Obs.-Calc. residuals for the rotational energies ($v = 0$) as a function of J , while Table 6 compares some residuals for $v = 0$ and $v = 1$.

Table 5. Example of Observed minus calculated R-branch frequencies as a function of J for the NS (0, 0) band.

J	+/-	Ω	Obs.	Calc.	Obs.-Calc.
0.5	+	0.5	2.3026	2.3024	0.0002
1.5	+	1.5	3.8760	3.8757	0.0003
2.5	+	0.5	5.3808	5.3806	0.0002
3.5	-	1.5	6.9758	6.9760	-0.0002
3.5	-	0.5	6.9198	6.9196	0.0002
4.5	+	1.5	8.5257	8.5259	-0.0002
5.5	+	0.5	10.0095	10.0098	-0.0003
6.5	+	0.5	11.5359	11.5356	0.0003

Table 6. Example of Observed – Calculated residuals for NS frequencies for various vibrational bands (R branch).

J	+/-	Ω	Band	Obs.	Calc.	Obs.-Calc.
0.5	+	0.5	(1, 0)	1206.5519	1206.5507	0.0012
1.5	-	1.5	(1, 0)	1207.9205	1207.9196	0.0008
2.5	+	0.5	(1, 0)	1209.5552	1209.5541	0.0011
3.5	-	0.5	(1, 0)	1211.0378	1211.0369	0.0009
4.5	+	0.5	(1, 0)	1212.5078	1212.5071	0.0007
5.5	-	0.5	(1, 0)	1213.9651	1213.9647	0.0005
6.5	+	0.5	(1, 0)	1215.4100	1215.4096	0.0004
7.5	-	1.5	(1, 0)	1216.7633	1216.7624	0.0009
8.5	+	0.5	(1, 0)	1218.2612	1218.2612	0.0000
9.5	+	0.5	(1, 0)	1219.6812	1219.6802	0.0010
10.5	+	1.5	(1, 0)	1221.0099	1221.0094	0.0005
11.5	+	1.5	(1, 0)	1222.3989	1222.3991	-0.0002
12.5	-	0.5	(1, 0)	1223.8239	1223.8231	0.0008
13.5	+	1.5	(1, 0)	1225.1387	1225.1391	-0.0004
14.5	-	1.5	(1, 0)	1226.4888	1226.4894	-0.0005
15.5	+	1.5	(1, 0)	1227.8262	1227.8265	-0.0003
17.5	-	0.5	(1, 0)	1230.4566	1230.4575	-0.0008
18.5	+	0.5	(1, 0)	1231.7462	1231.7477	-0.0015
20.5	+	1.5	(1, 0)	1234.3120	1234.3126	-0.0005
22.5	-	0.5	(1, 0)	1236.7884	1236.7888	-0.0004
24.5	+	1.5	(1, 0)	1239.2594	1239.2603	-0.0009
25.5	+	1.5	(1, 0)	1240.4629	1240.4637	-0.0008
28.5	-	0.5	(1, 0)	1243.9352	1243.9340	0.0012
30.5	-	1.5	(1, 0)	1246.2757	1246.2745	0.0012
32.5	+	0.5	(1, 0)	1248.4186	1248.4170	0.0015
34.5	-	0.5	(1, 0)	1250.5983	1250.5935	0.0048
2.5	-	0.5	(1, 1)	5.3493	5.3497	-0.0003
3.5	-	0.5	(1, 1)	6.8637	6.8634	0.0003
4.5	-	0.5	(1, 1)	8.4028	8.4025	0.0003
5.5	+	0.5	(1, 1)	9.9289	9.9287	0.0002
2.5	+	1.5	(2, 2)	5.3371	5.3368	0.0003
3.5	+	0.5	(2, 2)	6.8201	6.8194	0.0007
4.5	-	0.5	(2, 2)	8.3339	8.3331	0.0008
2.5	-	0.5	(3, 3)	5.2622	5.2609	0.0013
3.5	-	1.5	(3, 3)	6.8043	6.8032	0.0011
2.5	+	0.5	(4, 4)	5.2046	5.2031	0.0015
3.5	-	0.5	(4, 4)	6.6935	6.6914	0.0021

3 RESULTS AND DISCUSSION

3.1 Line lists

3.1.1 SH

Line lists for the five most important isotopologues of SH were computed using Duo. Table 7 summarises the statistics for these line lists. Those for SH contain almost 200,000 lines while the heavier D atom means that the ^{32}SD line list contains more than double this number of transitions. In order to further improve the numerical stability of intensity calculations for high overtones, we follow the procedure used by Wong et al. (2017) and apply a cutoff of 10^{-8} D to all matrix elements of the dipole moment $\langle v|\mu|v'\rangle$. The full line lists are given in the ExoMol format (Tennyson et al. 2016c) as supplementary data. Extracts of the states and transitions files are given in Tables 8 and 9 respectively. Apart from the energy term values,

Table 7. Statistics for the SH and NS line lists.

	³² SH	³³ SH	³⁴ SH	³⁶ SH	³² SD	¹⁴ N ³² S	¹⁴ N ³³ S	¹⁴ N ³⁴ S	¹⁴ N ³⁶ S	¹⁵ N ³² S
J_{\max}	60.5	60.5	60.5	60.5	84.5	235.5	236.5	237.5	239.5	240.5
number of energies	2326	2326	2328	2334	4532	31502	31802	32089	32620	33051
number of lines	81,348	81,274	81,319	81,664	219,463	2,755,796	2,795,487	2,831,482	2,901,113	2,957,016

Table 8. Extract from the states file of the ³²S¹H line list.

n	Energy (cm ⁻¹)	g_i	J	τ	g -factor	Parity	e/f	State	v	Λ	Σ	Ω
1	360.537424	4	0.5	inf	-0.000697	+	e	X2Pi	0	1	-0.5	0.5
2	2959.255407	4	0.5	0.708340	-0.000699	+	e	X2Pi	1	1	-0.5	0.5
3	5461.024835	4	0.5	0.247650	-0.000699	+	e	X2Pi	2	1	-0.5	0.5
4	7865.670867	4	0.5	0.130790	-0.000700	+	e	X2Pi	3	1	-0.5	0.5
5	10172.812283	4	0.5	0.083811	-0.000699	+	e	X2Pi	4	1	-0.5	0.5
6	12381.905056	4	0.5	0.060462	-0.000699	+	e	X2Pi	5	1	-0.5	0.5
7	14492.276445	4	0.5	0.047367	-0.000697	+	e	X2Pi	6	1	-0.5	0.5
8	16503.167217	4	0.5	0.039468	-0.000694	+	e	X2Pi	7	1	-0.5	0.5
9	18413.775027	4	0.5	0.034505	-0.000687	+	e	X2Pi	8	1	-0.5	0.5
10	20223.296263	4	0.5	0.031348	-0.000679	+	e	X2Pi	9	1	-0.5	0.5
11	21930.957245	4	0.5	0.029391	-0.000669	+	e	X2Pi	10	1	-0.5	0.5
12	23535.998338	4	0.5	0.028279	-0.000659	+	e	X2Pi	11	1	-0.5	0.5
13	25037.635167	4	0.5	0.027810	-0.000646	+	e	X2Pi	12	1	-0.5	0.5
14	26435.111738	4	0.5	0.027863	-0.000627	+	e	X2Pi	13	1	-0.5	0.5
15	27727.807976	4	0.5	0.028375	-0.000599	+	e	X2Pi	14	1	-0.5	0.5

n : State counting number.

\tilde{E} : State energy in cm⁻¹.

g_i : Total statistical weight, equal to $g_{\text{ns}}(2J+1)$.

J : Total angular momentum.

τ : Lifetime (s⁻¹).

g : Landé g -factors.

+/-: Total parity.

e/f: Rotationless parity.

State: Electronic state.

v : State vibrational quantum number.

Λ : Projection of the electronic angular momentum.

Σ : Projection of the electronic spin.

Ω : Projection of the total angular momentum, $\Omega = \Lambda + \Sigma$.

statistical weights and quantum numbers, the states file also contains the lifetimes (Tennyson et al. 2016a) and the Landé g -factors (Semenov et al. 2017).

3.1.2 NS

For NS, five line lists were computed for the isotopologues ¹⁴N³²S, ¹⁴N³³S, ¹⁴N³⁴S, ¹⁴N³⁶S and ¹⁵N³²S (see Table 7). The line lists are based in the lowest $v_{\max} = 60$ vibrational eigenfunctions with the rotational quantum number J ranging from 0.5 to 200.5 and the maximum energy term value E_{\max} was set from 0 cm⁻¹ to 38 964.6 cm⁻¹. The frequency window was set to 23 000 cm⁻¹ which is just below the next electronic state, $a^4\Pi$ (Gao et al. 2013). The values of v_{\max} and E_{\max} correspond to the dissociation limit of 4.83 eV determined by (Czernek & Živný 2004). A dipole moment cutoff of 10⁻⁸ D was also used. Again, Tables 10 and 11 show extracts from the corresponding states and transition files.

3.2 Partition Functions

Partition functions were computed up to 5000 K for every species considered at 1 K intervals. These can be found in the supplementary material. We have also fitted the partition function to the function form of Vidler & Tennyson (2000):

$$\log_{10} Q(T) = \sum_{n=0}^9 a_n (\log_{10} T)^n. \quad (7)$$

Table 12 gives the expansion coefficients for the parent isotopologues, fits for other species can be found in the supplementary material, which reproduce the ExoMol partition function within 2–3 %.

In general our partition functions are in excellent agreement with those available from other sources, namely from Sauval & Tatum (1984), Barklem & Collet (2016) and the CDMS database (Müller et al. 2005), once allowance is made for

Table 9. Extract from the transitions file of the ^{32}SH line list.

f	i	A_{fi} (s^{-1})	$\tilde{\nu}_{fi}$
1037	1051	5.28E-006	12167.591629
501	399	4.09E-006	12167.733027
1625	1633	1.56E-005	12168.620635
355	372	9.54E-006	12169.526762
868	828	7.14E-003	12170.134555
896	800	6.94E-003	12170.552236
1064	1024	4.92E-006	12170.716947
385	342	1.16E-005	12170.931908
175	252	1.27E-005	12171.792693
804	821	5.70E-007	12172.527689
205	222	1.29E-005	12172.803180
1528	1584	3.80E-004	12172.908871
1510	1520	1.61E-005	12173.738888
1552	1517	7.02E-006	12174.190774
620	520	7.76E-006	12174.773993
1551	1562	3.86E-004	12174.802908
112	69	1.58E-008	12174.960464
818	832	2.67E-005	12175.374485

f : Upper state counting number;
 i : Lower state counting number;
 A_{fi} : Einstein-A coefficient in s^{-1} ;
 $\tilde{\nu}_{fi}$: transition wavenumber in cm^{-1} .

Table 10. Extract from the states file for the line list of $^{14}\text{N}^{32}\text{S}$.

i	Energy (cm^{-1})	g_i	J	τ	g	Parity	e/f	State	v	Λ	Σ	Ω
1	0.000000	6	0.5	inf	-0.000767	+	e	X2Pi	0	1	-0.5	0.5
2	1204.267014	6	0.5	7.5810E-001	-0.000767	+	e	X2Pi	1	1	-0.5	0.5
3	2391.811399	6	0.5	3.7574E-001	-0.000767	+	e	X2Pi	2	1	-0.5	0.5
4	3562.543092	6	0.5	2.4892E-001	-0.000767	+	e	X2Pi	3	1	-0.5	0.5
5	4716.365128	6	0.5	1.8592E-001	-0.000767	+	e	X2Pi	4	1	-0.5	0.5
6	5853.187808	6	0.5	1.4840E-001	-0.000767	+	e	X2Pi	5	1	-0.5	0.5
7	6972.935476	6	0.5	1.2360E-001	-0.000767	+	e	X2Pi	6	1	-0.5	0.5
8	8075.513299	6	0.5	1.0604E-001	-0.000767	+	e	X2Pi	7	1	-0.5	0.5
9	9160.809357	6	0.5	9.3014E-002	-0.000767	+	e	X2Pi	8	1	-0.5	0.5
10	10228.711651	6	0.5	8.2993E-002	-0.000767	+	e	X2Pi	9	1	-0.5	0.5
11	11279.122350	6	0.5	7.5073E-002	-0.000767	+	e	X2Pi	10	1	-0.5	0.5
12	12311.955993	6	0.5	6.8677E-002	-0.000767	+	e	X2Pi	11	1	-0.5	0.5
13	13327.125579	6	0.5	6.3426E-002	-0.000767	+	e	X2Pi	12	1	-0.5	0.5
14	14324.536677	6	0.5	5.9056E-002	-0.000767	+	e	X2Pi	13	1	-0.5	0.5
15	15304.087622	6	0.5	5.5383E-002	-0.000767	+	e	X2Pi	14	1	-0.5	0.5
16	16265.666432	6	0.5	5.2272E-002	-0.000767	+	e	X2Pi	15	1	-0.5	0.5
17	17209.152585	6	0.5	4.9619E-002	-0.000767	+	e	X2Pi	16	1	-0.5	0.5
18	18134.433115	6	0.5	4.7350E-002	-0.000767	+	e	X2Pi	17	1	-0.5	0.5
19	19041.403694	6	0.5	4.5404E-002	-0.000767	+	e	X2Pi	18	1	-0.5	0.5
20	19929.953675	6	0.5	4.3734E-002	-0.000767	+	e	X2Pi	19	1	-0.5	0.5

i : State counting number.
 \tilde{E} : State energy in cm^{-1} .
 g : Total statistical weight, equal to $g_{\text{ns}}(2J+1)$.
 J : Total angular momentum.
 τ : Lifetime (s^{-1}).
 g : Landé g -factors.
 $+/-$: Total parity.
 e/f : Rotationless parity.
 State: Electronic state.
 v : State vibrational quantum number.
 Λ : Projection of the electronic angular momentum.
 Σ : Projection of the electronic spin.
 Ω : $\Omega = \Lambda + \Sigma$, projection of the total angular momentum.

Table 11. Extract from the transition file for the line list of $^{14}\text{N}^{32}\text{S}$.

f	i	A_{fi} (s^{-1})	$\tilde{\nu}_{fi}$
7738	7381	1.0816E-12	21129.956080
5205	5270	1.5211E-12	21129.964779
5098	5376	1.5212E-12	21129.965742
11335	11591	3.1996E-13	21129.967612
13834	13865	1.5996E-13	21129.972884
6281	5916	1.5599E-14	21129.973205
7633	7486	1.0819E-12	21129.974657
17595	17799	1.3308E-13	21130.010597
18641	18492	2.9298E-12	21130.032427
14941	14800	1.0700E-15	21130.038476
15071	14910	3.7284E-14	21130.042388
22202	21929	5.7979E-15	21130.049792
7889	7931	7.6269E-17	21130.090860
12655	12499	4.4455E-18	21130.105215
5327	5386	7.8126E-18	21130.120789
21381	21404	7.3821E-16	21130.145157
13229	12887	5.8001E-15	21130.148827
25770	25777	3.0568E-15	21130.159305
18726	18407	2.9242E-12	21130.204387
12449	12495	2.5432E-13	21130.208111
15334	15370	2.3191E-13	21130.223604

f : Upper state counting number;
 i : Lower state counting number;
 A_{fi} : Einstein-A coefficient in s^{-1} ;
 $\tilde{\nu}_{fi}$: transition wavenumber in cm^{-1} .

Table 12. Expansion coefficients for the partition function given by Eq. (7). Parameters for other isotopologues can be found in the supplementary material.

a_i	^{32}SH	$^{14}\text{N}^{32}\text{S}$
a_0	1.20403	1.10562
a_1	-0.47064	0.19180
a_2	2.88449	1.01142
a_3	-6.62867	-1.40930
a_4	7.73660	1.96534
a_5	-5.21848	-1.82956
a_6	2.16261	1.00323
a_7	-0.54158	-0.31160
a_8	0.07488	0.05081
a_9	-0.00437	-0.00338

the nuclear spin conventions employed: ExoMol uses the HITRAN convention which leads to a factor of 2 for ^{32}SH and 3 for $^{14}\text{N}^{32}\text{S}$ compared to the ‘astronomers’ convention employed by [Sauval & Tatum \(1984\)](#) and [Barklem & Collet \(2016\)](#). The only significant disagreement is for SH below 1000 K, where the results of [Sauval & Tatum \(1984\)](#) follow the wrong trend; [Sauval & Tatum \(1984\)](#) only aimed to be accurate above 1000 K.

Our partition functions should be complete up to 5000 K. For SH, the completeness is within 0.3 %, which corresponds to the number of states in our line list above the experimental dissociation energy ([Continetti et al. 1991](#)) at $T = 5000$ K. For NS, we mainly miss the contributions from the $a^4\Pi$ rovibronic states not considered here ($T_e = 24,524 \text{ cm}^{-1}$, [Gao et al. \(2013\)](#)). This should not exceed 1 % judging by the contribution to $Q(T)$ from the $X^2\Pi$ energies of NS above $24,524 \text{ cm}^{-1}$.

3.3 Spectra

3.3.1 SH

Figure 11 gives an overview of the spectrum of SH at different temperatures. Note how intensities drop exponentially across the entire frequency range shown: no unphysical, plateau-like structures at higher frequencies is present ([Medvedev et al. 2016](#)). This illustrates that our measures to prevent this spurious effect were successful. Figure 12 compares a simulated emission spectrum at $T = 2000$ K (HWHW = 0.01 cm^{-1}) to the experimental spectrum of [Winkel & Davis \(1984\)](#). The agreement is good, especially considering the complex coupling and the limited amount of the experimental data. Figure 13 shows a comparison of an SH spectrum at $T = 296$ K computed using the ExoMol line list with that from the CDMS

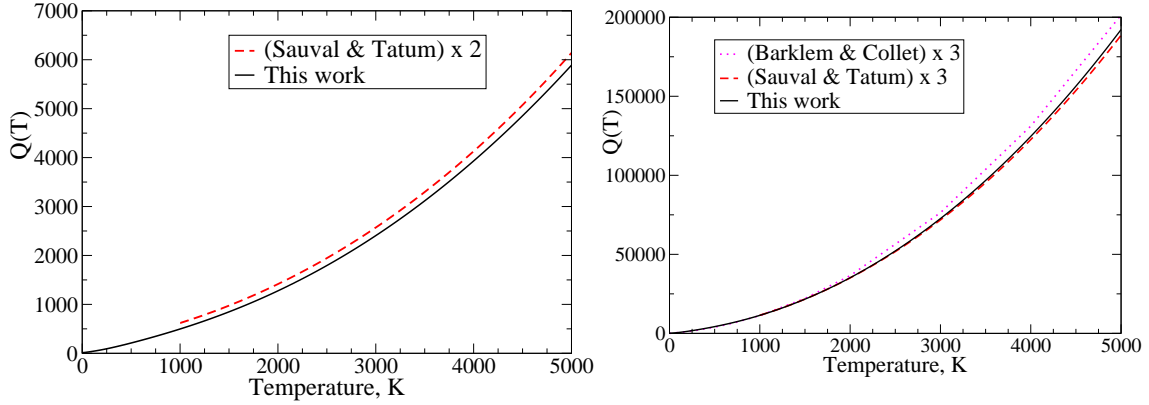


Figure 10. Temperature dependence of the partition functions of SH (left) and NS (right) computed using our line lists and compared to those by [Sauval & Tatum \(1984\)](#) and [Barklem & Collet \(2016\)](#).

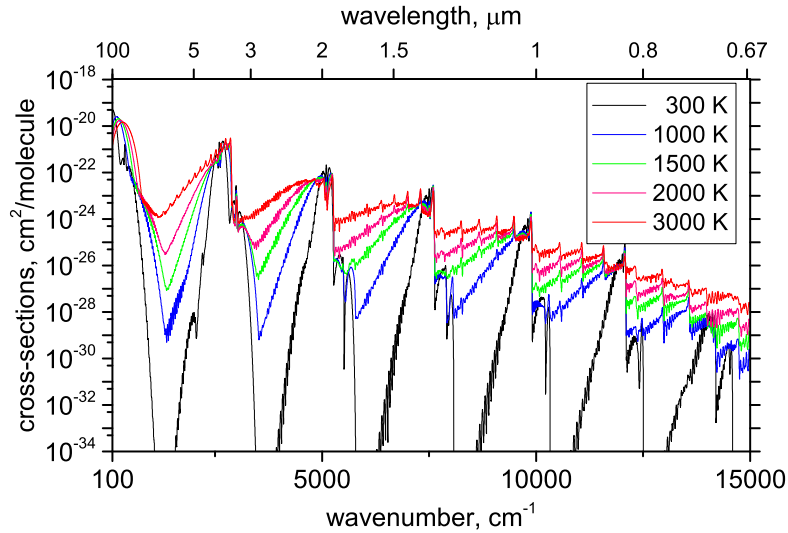


Figure 11. Temperature dependence of our simulated SH absorption spectrum. A Gaussian line profile with $\text{HWHM}=1 \text{ cm}^{-1}$ is used. The curves become flatter with increasing temperature.

database ([Müller et al. 2005](#)). The CDMS spectrum was obtained using the equilibrium dipole moment of 0.7580 D from [Meerts & Dymanus \(1974\)](#), while our value is 0.794 D.

3.3.2 NS

Figure 14 shows a comparison of spectra for the main isotopologue of NS as a function of temperature. Figure 15 shows the effects on the spectra of NS when the main isotopes of N and S are substituted. It can be seen that effect of substitution of the N atom leads to redshifts of up to 28 cm^{-1} and that of substituting S is up to 10 cm^{-1} .

To illustrate the accuracy of our line lists, spectra have been simulated and compared to the existing CDMS database ([Müller et al. 2005](#)) for the rotational and fundamental bands of NS, see Fig.16. In order to make this comparison, hyperfine splitting was averaged in the CDMS transitions of NS. Our intensities are in good agreement with those from CDMS. Some difference between the intensities from the fundamental band is due to the different *ab initio* dipole moments used: our transition dipole μ_1 for the fundamental band is 0.049 D, while CDMS used $\mu_1 = 0.045 \text{ D}$ from unpublished work by H. Müller.

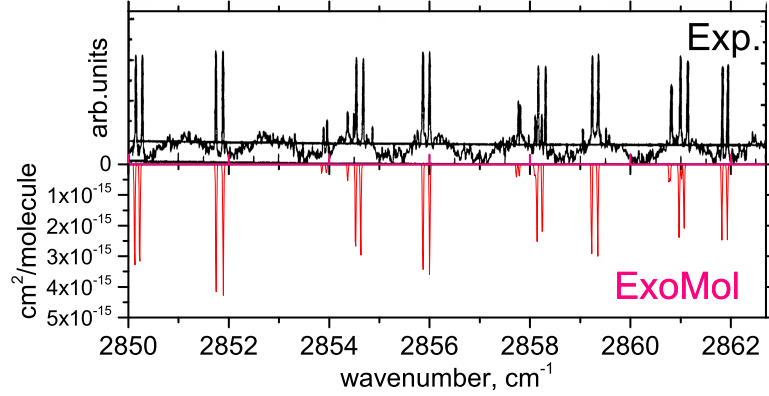


Figure 12. Comparison of simulated spectra at 2000 K (HWHM=0.01 cm⁻¹) using the new ExoMol line list for ³²SH and experimental spectra by Winkel & Davis (1984).

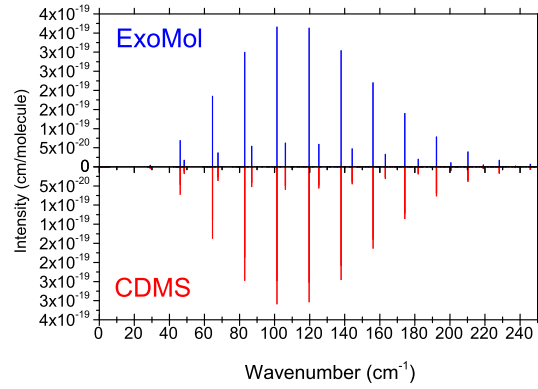


Figure 13. Comparison of simulated spectra using the new ExoMol line list for ³²SH and the CDMS database for the $\nu = 0$ band.

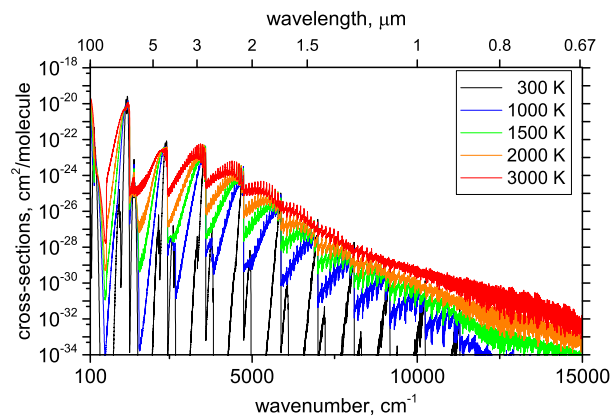


Figure 14. Temperature dependence of our simulated NS absorption spectrum. A Gaussian line profile with HWHM=1 cm⁻¹ is used. The curves become flatter with increasing temperature.

3.4 Lifetimes

Lifetimes for states within the $X^2\Pi$ ground state can be computed in straightforward manner from our line lists (Tennyson et al. 2016a). These are included in states file, see Tables 8 and 10 above. Figure 17 presents lifetimes states associated with the main isotopologues of SH and NS. As can be seen for NS, lifetimes for each vibrational state decrease by approximately up to one order of magnitude as energy is increased.

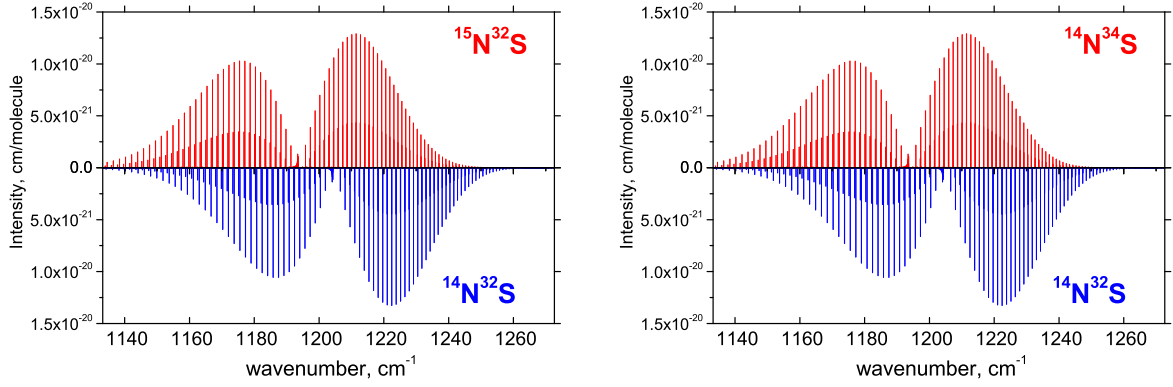
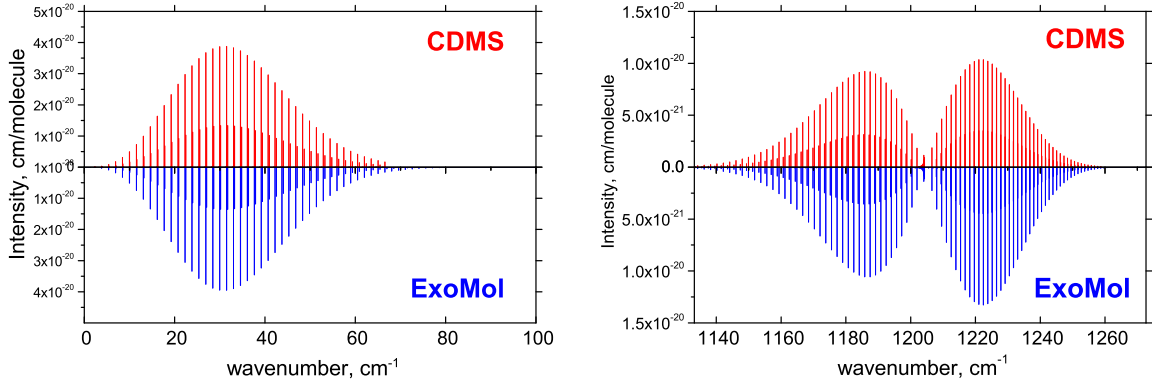


Figure 15. Comparison of spectra (298 K) for the fundamental $v = 1 - 0$ band of NS for $^{15}\text{N}^{32}\text{S}$ (left) and $^{14}\text{N}^{34}\text{S}$ (right) against $^{14}\text{N}^{32}\text{S}$.



[H]

Figure 16. Detailed Comparison our results with those given by CDMS (Müller et al. 2005) for pure rotational transitions (left) and the $v = 1 - 0$ fundamental band (right).

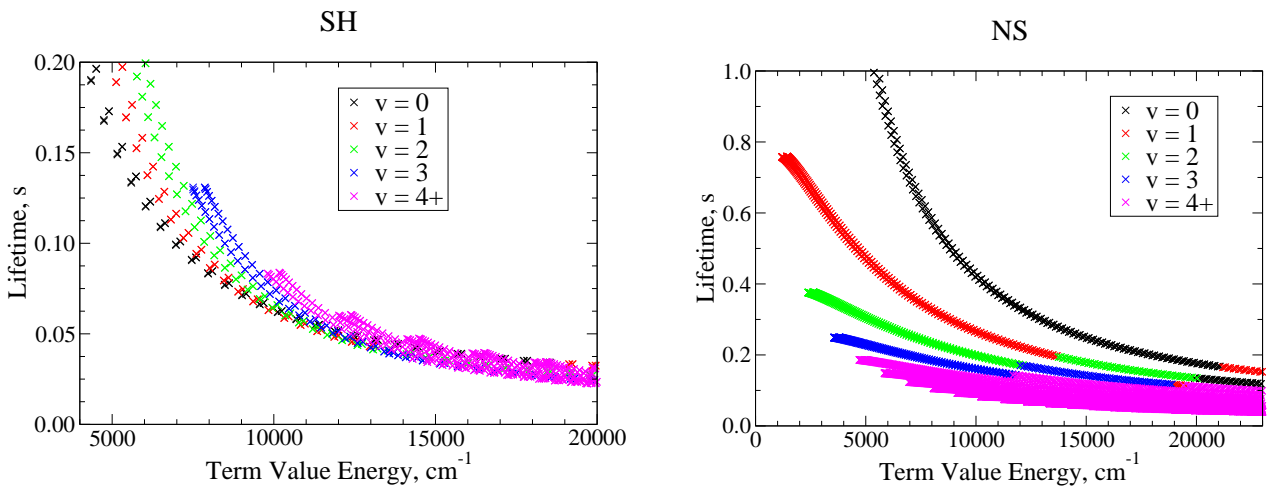


Figure 17. Lifetimes calculated for levels of ^{32}SH and $^{14}\text{N}^{32}\text{S}$ in their the $X^2\Pi$ electronic states. For SH the lifetimes increase with vibrational excitation; for NS the longest lived states are for $v = 0$ and the lifetimes decrease with vibrational excitation.

4 CONCLUSIONS

New line lists for the electronic ground states of major isotopologues of both SH and NS are generated using a high level *ab initio* theory refined to available experimental data. For SH, each line list contains approximately 81 000 transitions and 2300 states, with a range up to the dissociation limit of 29 234 cm⁻¹, vibrational coverage up to 14 and rotational coverage to $J = 60.5$. For NS, the line lists contain 2.7 – 2.9 million transitions up to 23 000 cm⁻¹ and 31 000 – 33 000 states with a range up to the dissociation limit of 38 964.6 cm⁻¹, with vibrational coverage up to $\nu=54$ and rotational coverage to $J = 235.5$. These are the only available hot line lists for these molecules. The line lists, which are named SNaSH, are available from the CDS (<http://cdsarc.u-strasbg.fr>) and ExoMol (www.exomol.com) data bases.

Our model is affected by the limitations of the experimental data as well as by the *ab initio* accuracy, especially for the dipole moment calculations. The latter is critical for accurate retrievals of molecular opacities in different astronomical bodies. It is typical for hot diatomics that experimental data on the dipole moments are either absent or extremely inaccurate, which emphasises the importance of the *ab initio* calculations of this property.

Considering the importance of the SH molecule for star spectroscopy, it would be important to extend the present study with the inclusion of the $A^2\Sigma^+$ electronic state, which would allow accurate modelling and prediction in the high-energy visible and UV spectral regions.

Our new line lists should enable detection of and inclusion in models of SH and NS for exoplanet temperatures which are largely not covered by experimental results. The ExoMol project has already provided line lists for several sulphur-containing molecules, namely CS (Paulose et al. 2015), SiS (Upadhyay et al. 2018), PS (Prajapat et al. 2017), H₂S (Azzam et al. 2016), SO₂ (Underwood et al. 2016a) and SO₃ (Underwood et al. 2016b). SO is probably the only major sulphur-bearing species which is important at elevated temperatures which is missing from this list.

5 ACKNOWLEDGEMENTS

This work was supported by the UK Science and Technology Research Council (STFC) No. ST/M001334/1 and the COST action MOLIM No. CM1405. This work made extensive use of UCL's Legion high performance computing facility.

REFERENCES

- Amano T., Saito S., Hirota E., Morino Y., 1969, *J. Mol. Spectrosc.*, 32, 97
 Anaconda J. R., 1994, *Spectra Chimica Acta A*, 50, 909
 Anaconda J. R., 1995, *Spectra Chimica Acta A*, 51, 39
 Anaconda J. R., Bogey M., Davies P. B., Demuyne C., Destombes J. L., 1986, *Mol. Phys.*, 59, 81
 Azzam A. A. A., Yurchenko S. N., Tennyson J., Naumenko O. V., 2016, *MNRAS*, 460, 4063
 Baeck K. K., Lee Y. S., 1990, *J. Chem. Phys.*, 93, 5775
 Barklem P. S., Collet R., 2016, *A&A*, 588, A96
 Belloche A., Müller H. S. P., Menten K. M., Schilke P., Comito C., 2013, *A&A*, 559, A47
 Benidar A., Farrenq R., Guelachvili G., Chackerian C., 1991, *J. Mol. Spectrosc.*, 147, 383
 Berdyugina S. V., Livingston W. C., 2002, *A&A*, 387, L6
 Bernath P. F., Amano T., Wong M., 1983, *J. Mol. Spectrosc.*, 98, 20
 Bialski M., Grein F., 1976, *J. Mol. Spectrosc.*, 61, 321
 Biver N., 2005, in Wilson A., ed., *ESA Special Publication Vol. 577*, ESA Special Publication. pp 151–156
 Brites V., Hammoutene D., Hochlaf M., 2008, *J. Phys.B: At. Mol. Phys.*, 41, 045101
 Brown J. M., Merer A. J., 1979, *J. Mol. Spectrosc.*, 74, 488
 Bruna P. J., Hirsch G., 1987, *Mol. Phys.*, 61, 1359
 Canaves M. V., de Almeida A. A., Boice D. C., Sanzovo G. C., 2002, *Earth Moon and Planets*, 90, 335
 Canaves M. V., de Almeida A. A., Boice D. C., Sanzovo G. C., 2007, *Adv. Space Res.*, 39, 451
 Carrington A., Howard B. J., Levy D. H., Robertson J. C., 1968, *Mol. Phys.*, 15, 187
 Charnley S. B., 1997, *ApJ*, 481, 396
 Continetti R. E., Balko B. A., Lee Y. T., 1991, *Chem. Phys. Lett.*, 182, 400
 Csaszar A. G., Leininger M. L., Burcat A., 2003, *J. Phys. Chem. A*, 107, 2061
 Czernek J., Živný O., 2004, *Chem. Phys.*, 303, 137
 Duley W. W., Millar T. J., Williams D. A., 1980, *MNRAS*, 192, 945
 Dunning Jr. T. H., 1989, *J. Chem. Phys.*, 90, 1007
 Eliet S., Martin-Drumel M.-A., Guinet M., Hindle F., Mouret G., Bocquet R., Cuisset A., 2011, *J. Mol. Spectrosc.*, 1006, 13
 Furtenbacher T., Császár A. G., Tennyson J., 2007, *J. Mol. Spectrosc.*, 245, 115
 Gao Y., Gao T., Gong M., 2013, *J. Quant. Spectrosc. Radiat. Transf.*, 129, 193
 Glockler G., Horwitz W., 1939, *J. Chem. Phys.*, 7, 857
 Gottlieb C. A., Ball J. A., Gottlieb E. W., Lada C. J., Penfield H., 1975, *ApJ*, 200, L147
 Heiles C. E., Turner B. E., 1971, *ApJL*, 8, 89
 Hirst D. M., Guest M. F., 1982, *Mol. Phys.*, 46, 427

- Irvine W. M., Lovell A. J., Senay M., Matthews H. E., Metz R. B., Meier R., McGonagle D., 1999, in AAS/Division for Planetary Sciences Meeting Abstracts #31. p. 32.03
- Karna S. P., Grein F., 1986, *J. Mol. Spectrosc.*, 120, 284
- Karpfen A., Schuster P., Petkov J., Lischka H., 1978, *J. Chem. Phys.*, 68, 3884
- Kashinski D. O., Talbi D., Hickman A. P., Di Nallo O. E., Colboc F., Chakrabarti K., Schneider I. F., Mezei J. Z., 2017, *J. Chem. Phys.*, 146, 204109
- Krishna Swamy K. S., Wallis M. K., 1987, *MNRAS*, 228, 305
- Krishna Swamy K. S., Wallis M. K., 1988, *A&AS*, 74, 227
- Lee E. G., Seto J. Y., Hirao T., Bernath P. F., Le Roy R. J., 1999, *J. Mol. Spectrosc.*, 194, 197
- Lee S. K., Ozeki H., Saito S., 1995, *ApJS*, 98, 351
- Leurini S., et al., 2006, *A&A*, 454, L47
- Lewis M. N., White J. U., 1939, *Phys. Rev.*, 55, 894
- Lie G. C., Peyerimhoff S. D., Buenker R. J., 1985, *J. Chem. Phys.*, 82, 2672
- Lodi L., Yurchenko S. N., Tennyson J., 2015, *Mol. Phys.*, 113, 1559
- Lovas F. J., Suenram R. D., 1982, *J. Mol. Spectrosc.*, 93, 416
- Lovas F. J., Johnson D. R., Snyder L. E., 1979, *ApJS*, 41, 451
- Martín S., 2005, in Hüttmeister S., Manthey E., Bomans D., Weis K., eds, AIP Conf. Ser. Vol. 783, The Evolution of Starbursts. pp 148–154, doi:10.1063/1.2034979
- Martin-Drumel M. A., Eliet S., Pirali O., Guinet M., Hindle F., Mouret G., Cuisset A., 2012, *Chem. Phys. Lett.*, 550, 8
- Martín S., Mauersberger R., Martín-Pintado J., García-Burillo S., Henkel C., 2003, *A&A*, 411, L465
- Martín S., Martín-Pintado J., Mauersberger R., Henkel C., García-Burillo S., 2005, *ApJ*, 620, 210
- Matsumura K., Kawaguchi K., Nagai K., Yamada C., Hirota E., 1980, *J. Mol. Spectrosc.*, 84, 68
- McCoy A. B., 1998, *J. Chem. Phys.*, 109, 170
- McGonagle D., Irvine W., Minh Y., 1992, in Singh P. D., ed., IAU Symposium Vol. 150, Astrochemistry of Cosmic Phenomena. p. 227
- McGonagle D., Irvine W. M., Ohishi M., 1994, *ApJ*, 422, 621
- McKemmish L. K., Yurchenko S. N., Tennyson J., 2016, *MNRAS*, 463, 771
- Medvedev E. S., Meshkov V. V., Stolyarov A. V., Ushakov V. G., Gordon I. E., 2016, *J. Mol. Spectrosc.*, 330, 36
- Meeks M. L., Gordon M. A., Litvak M. M., 1969, *Science*, 163, 173
- Meerts W. L., Dymanus A., 1974, *ApJ*, 187, L45
- Meier D. S., et al., 2015, *ApJ*, 801, 63
- Meuwly M., Hutson J. M., 1999, *J. Chem. Phys.*, 110, 8338
- Müller H. S. P., Schlöder F., Stutzki J., Winnewisser G., 2005, *J. Molec. Struct. (THEOCHEM)*, 742, 215
- Narasimham N. A., Balasubramanian T. K., 1971, *J. Mol. Spectrosc.*, 40, 511
- Neufeld D. A., et al., 2012, *A&A*, 542, L6
- Oppenheimer M., Dalgarno A., 1974, *ApJ*, 187, 231
- Patrascu A. T., Tennyson J., Yurchenko S. N., 2015, *MNRAS*, 449, 3613
- Paulose G., Barton E. J., Yurchenko S. N., Tennyson J., 2015, *MNRAS*, 454, 1931
- Peterson K. A., Dunning Jr. T. H., 2002, *J. Chem. Phys.*, 117, 10548
- Prajapat L., Jagoda P., Lodi L., Gorman M. N., Yurchenko S. N., Tennyson J., 2017, *MNRAS*, 472, 3648
- Qui-Xia L., Tao G., Yun-Guang Z., 2008, *Chin. Phys. B*, 17, 2040
- Raimondi M., Tantardini G. F., Simonetta M., 1975, *Mol. Phys.*, 30, 703
- Ram R. S., Bernath P. F., Engleman R., Brault J. W., 1995, *J. Mol. Spectrosc.*, 172, 34
- Ravichandran K., Williams R., Fletcher T. R., 1994, *Chem. Phys. Lett.*, 217, 375
- Resende S. M., Ornellas F. R., 2001, *J. Chem. Phys.*, 115, 2178
- Rodgers S. D., Charnley S. B., 2006, *Adv. Space Res.*, 38, 1928
- Salahub D. R., Messmer R. P., 1976, *J. Chem. Phys.*, 64, 2039
- Sauval A. J., Tatum J. B., 1984, *ApJS*, 56, 193
- Semenov M., Yurchenko S. N., Tennyson J., 2017, *J. Mol. Spectrosc.*, 330, 57
- Shi D. H., Xing W., Sun J. F., Zhu Z. L., 2012, *Eur. Phys. J. D*, 66, 173
- Sinha A., Burkholder J. B., Hammer P. D., Howard C. J., 1988, *J. Mol. Spectrosc.*, 130, 466
- Skokov S., Peterson K. A., Bowman J. M., 1999, *Chem. Phys. Lett.*, 312, 494
- Somerville W. B., 1977, *Rep. Prog. Phys.*, 40, 483
- Szalay P., Müller T., Gidofalvi G., Lischka H., Shepard R., 2012, *Chem. Rev.*, 112, 108
- Tennyson J., Hulme K., Naim O. K., Yurchenko S. N., 2016a, *J. Phys. B: At. Mol. Opt. Phys.*, 49, 044002
- Tennyson J., Lodi L., McKemmish L. K., Yurchenko S. N., 2016b, *J. Phys. B: At. Mol. Opt. Phys.*, 49, 102001
- Tennyson J., et al., 2016c, *J. Mol. Spectrosc.*, 327, 73
- Uehara H., Morino Y., 1969, *Mol. Phys.*, 17, 239
- Underwood D. S., Tennyson J., Yurchenko S. N., Huang X., Schwenke D. W., Lee T. J., Clausen S., Fateev A., 2016a, *MNRAS*, 459, 3890
- Underwood D. S., Tennyson J., Yurchenko S. N., Clausen S., Fateev A., 2016b, *MNRAS*, 462, 4300
- Upadhyay A., Conway E. K., Tennyson J., Yurchenko S. N., 2018, *MNRAS*
- Vamhindi B. S. D. R., Nsangou M., 2016, *Mol. Phys.*, 114, 2204
- Vidal T. H. G., Loison J.-C., Jaziri A. Y., Ruaud M., Gratier P., Wakelam V., 2017, *MNRAS*, 469, 435
- Vidler M., Tennyson J., 2000, *J. Chem. Phys.*, 113, 9766
- Visscher C., Lodders K., Fegley Jr. B., 2006, *ApJ*, 648, 1181
- Werner H.-J., Knowles P. J., Knizia G., Manby F. R., Schütz M., 2012, *WIREs Comput. Mol. Sci.*, 2, 242
- Western C. M., 2017, *J. Quant. Spectrosc. Radiat. Transf.*, 186, 221
- Winkel R. J., Davis S. P., 1984, *Can. J. Phys.*, 62, 1420

- Wong A., Yurchenko S. N., Bernath P., Mueller H. S. P., McConkey S., Tennyson J., 2017, [MNRAS](#), 470, 882
Woods P. M., Occhiogrosso A., Viti S., Kaňuchová Z., Palumbo M. E., Price S. D., 2015, [MNRAS](#), 450, 1256
Woon D. E., Dunning T. H., 1993, *J. Chem. Phys.*, 98, 1358
Yamamura I., Kawaguchi K., Ridgway S. T., 2000, [ApJ](#), 528, L33
Yurchenko S. N., Lodi L., Tennyson J., Stolyarov A. V., 2016a, [Comput. Phys. Commun.](#), 202, 262
Yurchenko S. N., Blissett A., Asari U., Vasilios M., Hill C., Tennyson J., 2016b, [MNRAS](#), 456, 4524
Yurchenko S. N., Sinden F., Lodi L., Hill C., Gorman M. N., Tennyson J., 2018, [MNRAS](#), 473, 5324
Zahnle K., Marley M. S., Freedman R. S., Lodders K., Fortney J. J., 2009, [Astrophys. J. Lett.](#), 701, L20
Zhao D., Galazutdinov G. A., Linnartz H., Krełowski J., 2015, [A&A](#), 579, L1